Progress In Electromagnetics Research B, Vol. 55, 195–215, 2013

A NEW IMAGING ALGORITHM FOR GEOSYNCHRONOUS SAR BASED ON THE FIFTH-ORDER DOPPLER PARAMETERS

Bingji Zhao[1, *], Yunzhong Han[1], Wenjun Gao[1], Yunhua Luo[2], and Xiaolei Han[2]

[1]Beijing Institute of Spacecraft System Engineering, Beijing 100094, The People's Republic of China

[2]Department of Space Microwave Remote Sensing System, Institute of Electronic, Chinese Academy of Science, Beijing 100190, The People's Republic of China

Abstract—This paper proposes a new imaging algorithm based on a novel accurate range model to process the data acquired by Geosynchronous-Earth-orbital Synthetic Aperture Radar (Geo-SAR). The new range model, called DRM-5, is obtained from the 1–5th order Doppler parameters of spaceborne SAR. It is employed to describe the slant range of Geo-SAR during the super-long integration time. Furthermore, the two-dimensional frequency spectrum of point targets based on the new range model is derived and analyzed. An advanced Frequency Domain Algorithm (FDA) based on DRM-5 is proposed to process the data of stripmap mode Geo-SAR. The varied Doppler parameters in the cross-azimuth direction are considered in the new imaging algorithm, and the space-varied range-azimuth coupling phase term is compensated through data blocking. A simulation experiment is performed to verify the efficiency and superiority of the new algorithm, and the results show that it has a good effect on an L-band stripmap mode Geo-SAR system with azimuth resolution around 5 m and 300 km range swath.

1. INTRODUCTION

Many new ideas about spaceborne SAR have been developed recently, and one of the most exciting is Geosynchronous-Earth-orbital SAR (Geo-SAR), firstly proposed by Tomiyasu in 1978 [1]. The orbital

Received 28 July 2013, Accepted 22 September 2013, Scheduled 2 October 2013

* Corresponding author: Bingji Zhao (zachary_zbj@163.com).

height of Geo-SAR is around 35,792 km, absolutely different from the traditional Low-Earth-Orbital SAR (Leo-SAR) systems whose orbital altitudes are lower than 1,000 km. A Geo-SAR system exhibits distinctive advantages which provide a large instantaneous field of view with a short repeat cycle equal to one Earth day [1–9].

A main problem of Geo-SAR is the super-long integration time, which is up to 30 min in some orbital positions, to traverse the long non-linear synthetic aperture distance. This property is quite different from Leo-SAR. Consequently, the traditional Hyperbolic Range equation (HRE) can never been used to describe the actual slant range between sensor and target in Geo-SAR condition. Therefore, a Taylor series range equation is employed to handle this problem in this paper. It is named as Doppler parameter Range Model (DRM), because the coefficients of the Taylor series range equation are essentially determined by the corresponding Doppler parameters. As a result, the phase error of DRM, compared with the actual slant range, is very small (under $\pi/4$) and has a good effect on Geo-SAR data processing and high resolution Leo-SAR imaging [10–13].

A new data focusing algorithm for a large scene of stripmap mode Geo-SAR system, performed by the 1–5th order Doppler parameters (DRM-5), is proposed in this paper. The accurate calculation approach of the 1–4th order Doppler parameters has been reported in [14] and [15], and that of the fifth-order Doppler parameter is presented in this paper.

The Range Doppler Algorithm (RDA), Chirp Scaling Algorithm (CSA) and ωK Algorithm (ωKA) are designed for high resolution processing of spaceborne SAR data. They are all designed based on HRE and can get a good focusing effect on Leo-SAR [16–20]. The traditional RDA is based on HRE, which cannot be applied to Geo-SAR imaging directly, but some ideas of the new algorithm in this manuscript come from it. In this paper, the point target two-dimensional Reference Frequency Spectrum (2D RFS) of DRM-n is derived at first and the spectrum is then expanded and analyzed. Finally, a new Frequency Domain Algorithm (FDA) based on DRM-5 is proposed.

This paper is structured as follows. In Section 2, the orbital properties of Geo-SAR and Leo-SAR are compared. The DRM-5 is illuminated, and the two-dimensional point target frequency spectrum is derived. The frequency spectrum is then expanded and analyzed. In Section 3, the new FDA is described. The simulation results are given in Section 4. The conclusion is finally proposed in Section 5.

2. SPACEBORNE SAR GEOMETRY AND DRM-n

2.1. Spaceborne SAR Geometry

The received signal of one single point target by a spaceborne SAR, demodulated into baseband, can be represented as:

$$S_r(\tau,\eta) = A_0\omega_r\left(\tau-\frac{2R(\eta)}{c}\right)\omega_a(\eta-\eta_c)\exp\left\{-j4\pi\frac{R(\eta)}{\lambda}\right\} \exp\left\{j\pi K_r\left(\tau-\frac{2R(\eta)}{c}\right)^2\right\} \quad (1)$$

where K_r is the range chirp rate, c the velocity of light, λ the wavelength, τ the fast time, η the slow time, η_c the beam center crossing time, A_0 a constant, $\omega_a(\cdot)$ defined by azimuth antenna pattern, and $\omega_r(\cdot)$ the range antenna pattern [5]. The slant range $R(\eta)$ is the most important parameter in data processing and can be accurately calculated by:

$$R(\eta) = \sqrt{(X_t(\eta)-x_s(\eta))^2+(Y_t(\eta)-y_s(\eta))^2+(Z_t(\eta)-z_s(\eta))^2} \quad (2)$$

where $X_t(\eta)$, $Y_t(\eta)$ and $Z_t(\eta)$ are the coordinates of the target in three-dimensional space during the integration time, and $x_s(\eta)$, $y_s(\eta)$ and $z_s(\eta)$ represent those of the satellite. We have built an accurate spaceborne SAR geometry to calculate the precise values of $R(\eta)$ in [14, 15]. The trace property of Geo-SAR is quite different from that of Leo-SAR. Fig. 1(a) shows their trajectories in Earth Centered Rotating (ECR) coordinates for comparison.

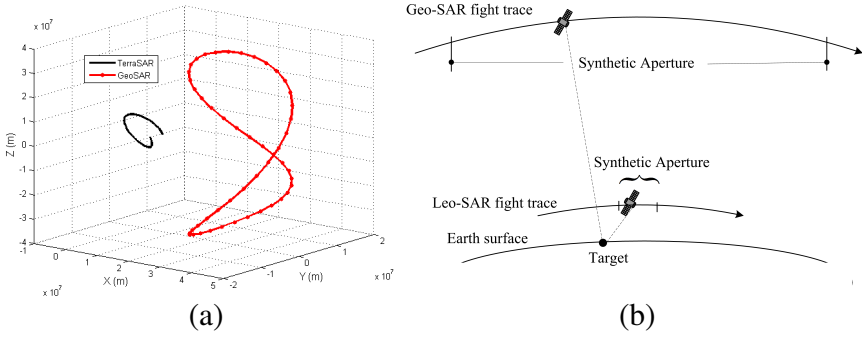

Figure 1. Geometry comparison between Geo-SAR and Leo-SAR in ECR. (a) Satellite's trajectory. (b) Synthetic aperture of spaceborne SAR.

The synthetic aperture of Geo-SAR is a long non-linear one due to its super-long integration time. In contrast, that of Leo-SAR is much shorter and can be considered as linear. The difference between them is approximately shown in Fig. 1(b). The slant range values $R(\eta)$ during integration time, calculated by Equation (2), can be described by the so-called range equation (range model). A hyperbolic model, HRE, is derived under the condition that a sensor's trajectory is assumed to be locally circular and that the Earth is considered as locally spherical and not rotating [5].

$$R_{\mathrm{HRE}}(\eta) = \sqrt{R_c^2 + V_r^2\eta^2 - 2R_cV_r\sin\theta_r\eta} \tag{3}$$

where R_c is the slant range of beam centerline, V_r the effective satellite velocity, and θ_r the effective squint angle. Equation (3) has the same form as the airborne SAR condition. A novel approach to improve its accuracy, depending on precise Doppler centroid and Doppler FM rate values, has been presented in [21]. However, it is still appropriate only for Leo-SAR with moderate resolution. A Geo-SAR system needs super-long exposure time to obtain high resolution, and the error of $R_{\mathrm{HRE}}(\eta)$, compared with $R(\eta)$, is very large. As a result, the rotating of the ellipsoidal Earth and the orbital eccentricity should be accurately analyzed to build the 'Satellite-target' geometry.

2.2. DRM-n

A new accurate range equation, referred to as DRM, has the capability to process data acquired in the super-long integration time for Geo-SAR. The nth-order DRM (DRM-n) can be described as:

$$\begin{cases} R_{\mathrm{DRM}}(\eta) = R_c + \sum\limits_{n=1}^{\infty} k_n(\eta-\eta_c)^n \\ k_1 = -\frac{\lambda}{2}f_{dc}, \quad k_{n+1} = -\frac{\lambda}{2(n+1)!}f_{nr}, \quad (n = 1, 2, \ldots) \end{cases} \tag{4}$$

where f_{dc} is the Doppler centroid and f_{nr} the nth-order Doppler FM rate. Its accuracy depends on the order number and the precision of Doppler parameters. This paper discusses the DRM determined by the 1st–5th order Doppler parameters (DRM-5). An accurate approach about the 1st–4th order Doppler parameter calculation for Geo-SAR has been introduced in [14] and [15], and the fifth order Doppler parameter can be written as:

$$\begin{aligned} f_{4r} \;=\; & -\frac{2}{\lambda}\left[\frac{10(\mathbf{A}_s-\mathbf{A}_t)\,(\mathbf{A}_s'-\mathbf{A}_t')}{r} + \frac{5(\mathbf{v}_s-\mathbf{v}_t)\,(\mathbf{A}_s''-\mathbf{A}_t'')}{r}\right. \\ & \left. + \frac{(\mathbf{r}_s-\mathbf{r}_t)\left(\mathbf{A}_s^{(3)}-\mathbf{A}_t^{(3)}\right)}{r} - \frac{10\lambda^2 f_{1r}f_{2r}}{4r} - \frac{5\lambda^2 f_{dc}f_{3r}}{4r}\right] \end{aligned} \tag{5}$$

where r is the distance between sensor and radar beam center line target, and $\mathbf{r}$, $\mathbf{v}$, $\mathbf{A}$, $\mathbf{A}'$, $\mathbf{A}''$ and $\mathbf{A}^{(3)}$ respectively denote the state vectors of position, velocity, acceleration, rate of acceleration, the second derivative of acceleration and the third derivative of acceleration. The DRM-5 achieves better accuracy than HRE since it can describe the satellite's curved path and fit an actual Geo-SAR system in stripmap mode.

The point target 2D RFS of DRM-5 will be derived rigorously to develop an efficient imaging algorithm in Section 3. Using the Principle of Stationary Phase (POSP) to obtain the range Fourier Transforming (FT) of expression (1), we can get:

$$\begin{aligned} S_r(f_\tau, \eta) &= A_1 W_r(f_\tau) \omega_a(\eta - \eta_c) \\ &\quad \exp\left\{-j\left[\frac{\pi f_\tau^2}{K_r} + \frac{4\pi(f_0 + f_\tau) R_{\mathrm{DRM}}(\eta)}{c}\right]\right\} \end{aligned} \tag{6}$$

where f_τ is the range frequency, f_0 the carrier frequency, $W_r(f_\tau)$ the envelope of the range frequency spectrum, and A_1 a constant. Furthermore, the signal is transformed into a two-dimensional frequency domain by azimuth FT.

$$S_r(f_\tau, f_\eta) = \int_{-\infty}^{+\infty} S_r(f_\tau, \eta) \exp\left\{-j2\pi f_\eta \eta\right\} d\eta \tag{7}$$

where f_η is the azimuth frequency. Using POSP, the relationship between azimuth frequency f_η and azimuth time η can be written as:

$$-\left[\frac{c f_\eta}{2\left(f_0 + f_\tau\right)} + k_1\right] = \sum_{n=1}^{\infty} \left(n+1\right) k_{n+1} \eta^n \tag{8}$$

According to the theory of Series Reversion (SR) proposed in [12], we can get:

$$\eta(f_\eta) = \sum_{n=1}^{\infty} (-1)^n P_n \left(\frac{c f_\eta}{2\left(f_0 + f_\tau\right)} + k_1\right)^n \tag{9}$$

where P_n can be derived based on the theory of SR. Substituting expression (9) into (7), we can obtain the two-dimensional point target frequency spectrum.

$$S_r(f_\tau, f_\eta) = A_2 W_r(f_\tau) W_a(f_\eta) \exp\left[j\Theta_n(f_\tau, f_\eta)\right] \tag{10}$$

where $W_r(f_\eta)$ is the envelope of the azimuth frequency spectrum, and A_2 is a constant. The phase term in (10) is represented by:

$$\Theta_n(f_\tau, f_\eta) = -\frac{\pi f_\tau^2}{K_r} - 2\pi f_\eta \eta(f_\eta) - \frac{4\pi\left(f_0 + f_\tau\right) R_{\mathrm{DRM}}\left[\eta(f_\eta)\right]}{c} \tag{11}$$

Substituting (9) into (11), we can obtain:

$$\Theta_n(f_\tau, f_\eta) = -\frac{\pi f_\tau^2}{K_r} - \frac{4\pi(f_0+f_\tau)}{c} \left\{R_c - \sum_{n=1}^{\infty}(-1)^{n+1}\frac{P_n}{n+1}\left[\frac{cf_\eta}{2(f_0+f_\tau)}+k_1\right]^{n+1}\right\} \quad (12)$$

Equations (10) and (12) represent the n-th order point target 2D RFS of DRM-n. It is evident that no approximation has been made in the aforementioned derivation, so it is an accurate representation of signal spectrum of DRM-n. The accuracy of the spectrum is decided by the number of orders. We discuss DRM-5 in this paper to get a good focusing result for a Geo-SAR system in stripmap mode, and its spectrum phase is:

$$\Theta_5(f_\tau, f_\eta) = -\frac{\pi f_\tau^2}{K_r} - \frac{4\pi(f_0+f_\tau)\left(R_c - \frac{P_1}{2}M^2 - \frac{P_2}{3}M^3 - \frac{P_3}{4}M^4 - \frac{P_4}{5}M^5\right)}{c} \quad (13)$$

where $M = -[cf_\eta/2(f_0+f_\tau)+k_1]$, $P_1 = 1/2k_2, P_2 = -3k_3/8k_2^3$, $P_3 = (9k_3^2 - 4k_2k_4)/16k_2^5$, $P_4 = -(135k_3^3 - 120k_2k_3k_4 + 20k_2^2k_5)/128k_2^7$.

The terms higher than the 5th order are neglected in expression (13). The point target 2D RFS may have a good focusing result on one single point target in the reference position of a scene; however, an efficient imaging algorithm for big scene should be advanced. To make an in-depth analysis of the phase term, the expression (13) is rearranged as:

$$\begin{aligned}\Theta_5(f_\tau, f_\eta) = &-\frac{\pi f_\tau^2}{K_r} - \frac{4\pi R_c}{\lambda} - \frac{4\pi R_c f_\tau}{c} + \frac{\pi\lambda P_1}{2}\left(1+\frac{f_\tau}{f_0}\right)^{-1}N^2 \\ &-\frac{\pi\lambda^2 P_2}{6}\left(1+\frac{f_\tau}{f_0}\right)^{-2}N^3 + \frac{\pi\lambda^3 P_3}{16}\left(1+\frac{f_\tau}{f_0}\right)^{-3}N^4 \\ &-\frac{\pi\lambda^4 P_4}{40}\left(1+\frac{f_\tau}{f_0}\right)^{-4}N^5 \end{aligned} \quad (14)$$

where $N = [(f_\eta - f_{dc}) - f_{dc}(f_\tau/f_0)]$. The $(1+f_\tau/f_0)^{-m}$ items in (14) can be expanded into a power series about f_τ, and the orders higher than the 4th are ignored. After series of complicated derivation, the phase term $\Theta_5(f_\tau, f_\eta)$ can then be decomposed into four parts as follows:

$$\Theta_5(f_\tau, f_\eta) = \Theta_r(f_\tau) + \Theta_{\mathrm{RCM}}(f_\tau, f_\eta) + \Theta_a(f_\eta) + \Theta_c(f_\tau, f_\eta) \quad (15)$$

where

$$\Theta_r(f_\tau) = -\frac{\pi f_\tau^2}{K_r} \tag{16}$$

$$\begin{aligned}\Theta_{\mathrm{RCM}}(f_\tau, f_\eta) = & -\frac{4\pi}{c}\cdot\left\{R_c + \frac{\lambda^2 P_1}{8}\left[(f_\eta - f_{dc})^2 + 2f_{dc}(f_\eta - f_{dc})\right]\right. \\ & -\frac{\lambda^3 P_2}{24}\left[2(f_\eta - f_{dc})^3 + 3f_{dc}(f_\eta - f_{dc})^2\right] \\ & +\frac{\lambda^4 P_3}{64}\left[3(f_\eta - f_{dc})^4 + 4f_{dc}(f_\eta - f_{dc})^3\right] \\ & \left.-\frac{\lambda^5 P_4}{160}\left[4(f_\eta - f_{dc})^5 + 5f_{dc}(f_\eta - f_{dc})^4\right]\right\}\cdot f_\tau \end{aligned} \tag{17}$$

$$\begin{aligned}\Theta_a(f_\eta) = & -\frac{4\pi R_c}{\lambda} + \frac{\pi\lambda P_1}{2}(f_\eta - f_{dc})^2 - \frac{\pi\lambda^2 P_2}{6}(f_\eta - f_{dc})^3 \\ & +\frac{\pi\lambda^3 P_3}{16}(f_\eta - f_{dc})^4 - \frac{\pi\lambda^4 P_4}{40}(f_\eta - f_{dc})^5 \end{aligned} \tag{18}$$

$$\Theta_c(f_\tau, f_\eta) = C_2 f_\tau^2 + C_3 f_\tau^3 \tag{19}$$

where $\Theta_r(f_\tau)$ is the range chirp, $\Theta_{\mathrm{RCM}}(f_\tau,\ f_\eta)$ the Range Cell Migration (RCM), $\Theta_a(f_\eta)$ the azimuth modulation and $\Theta_c(f_\tau,$ and $f_\eta)$ the signal's range/azimuth coupling term. Two parts of the coupling phase term $\Theta_c(f_\tau,\ f_\eta)$ are shown in this manuscript: one is a quadratic term about f_τ, and the other is a cubic term. They are both significant for Geo-SAR data processing, and the other terms are omitted here. The corresponding coefficients of the two terms are shown as follows.

$$\begin{cases} C_2 = \frac{\pi f_\eta^2}{f_0^2}\left\{\frac{\lambda P_1}{2} - \frac{\lambda^2 P_2}{2}(f_\eta - f_{dc}) + \frac{3\lambda^3 P_3}{8}(f_\eta - f_{dc})^2 - \frac{\lambda^4 P_4}{4}(f_\eta - f_{dc})^3\right\} \\ C_3 = -\frac{\pi f_\eta^2}{f_0^3}\left\{\frac{\lambda P_1}{2} - \frac{\lambda^2 P_2}{6}\left[4(f_\eta - f_{dc}) + f_{dc}\right] + \frac{\lambda^3 P_3}{16}\left[10(f_\eta - f_{dc})^2\right.\right. \\ \qquad \left.\left. + 4f_{dc}(f_\eta - f_{dc})\right] - \frac{\lambda^4 P_4}{32}\left[16(f_\eta - f_{dc})^3 + 8f_{dc}(f_\eta - f_{dc})^2\right]\right\} \end{cases}$$

The point target 2D RFS of DRM-5 is given by expressions (10) and (15). To analyze conveniently, the phase term has been expanded and presented by Equations (16)–(19). It is derived in the general case that the satellite's attitude has not been controlled. If the two-dimensional attitude steering (yaw steering and pitch steering) has been performed, the Doppler centroid f_{dc} is zero, and the other four Doppler parameters will also change [15, 22]. Since the 1st–5th Doppler parameters can be accurately calculated, the proposed DRM5 enjoys high accuracy. In fact, this theory is not only fit for Geo-SAR, but also effective for high resolution Leo-SAR.

3. FREQUENCY DOMAIN ALGORITHM FOR STRIPMAP MODE GEO-SAR

A Geo-SAR system, at an altitude around 35,792 km, needs a large physical antenna to provide the great deal of transmitted power. This paper discusses an L-Band Geo-SAR system with a 30 m diameter aperture antenna working in the Stripmap mode. Since no Geo-SAR system has been launched yet, a raw echo signal is simulated by Equation (1), and the slant range is calculated by expression (2). This method will be credible. The simulation parameters are listed in Table 1.

The classic RDA is efficient to achieve block processing in both range and azimuth frequency domain, while maintaining the simplicity of one-dimensional operations. However, it is based on the frequency spectrum from HRE and is not capable of processing Geo-SAR data.

Table 1. Simulation parameters for Geo-SAR.

Name	**Value**
Orbital altitude (km)	35792
Eccentricity	0.0011
Longitude ascending node (°)	0
perigee argument (°)	90
Inclination (°)	60
Earth model	WGS-84
Range swath width (km)	300
Center elevation angle (°)	7.3
Scene latitude/longitude (°)	30.2/42.1
Name	**Value**
Exposure time (s)	620
Antenna size (m)	30
Wavelength (m)	0.24
Bandwidth (MHz)	31
Azimuth resolution (m)	5
Range resolution (m)	5
Chip duration (μs)	50
Pulse repetition frequency (Hz)	60
Attitude steering or not	Yes

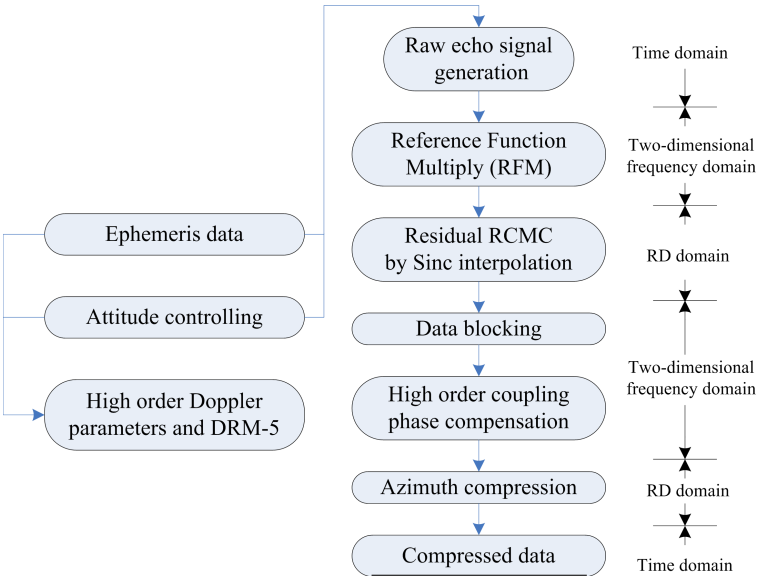

Figure 2. Block diagram of FDA based on DRM-5 for stripmap mode Geo-SAR.

A new Frequency domain Algorithm (FDA) is proposed based on the point target 2D RFS of DRM-5 derived in Section 2. The key processing operations of FDA are performed in both RD domain and wave number domain, thus it can be considered as a hybrid algorithm. Fig. 2 shows a block diagram of FDA based on DRM-5.

Firstly, the raw signal data is transformed into the wave number domain by two-dimensional FFT, and the Reference Function Multiply (RFM) is performed then. The target located at the scene center is defined as the reference one, and its slant range is taken as reference slant range. The expression of the reference function is written as:

$$H_{\mathrm{RFM}}(f_\tau, f_\eta) = \exp\left\{ j\frac{\pi f_\tau^2}{K_r} + j\frac{4\pi(f_0+f_\tau)}{c}\left(R_r - \frac{P_{1r}}{2}M_r^2 - \frac{P_{2r}}{3}M_r^3 - \frac{P_{3r}}{4}M_r^4 - \frac{P_{4r}}{5}M_r^5 \right) \right\} \tag{20}$$

where the subscript r means "*ref*". Using the RFM filter compensates the phase of the reference target, including the range frequency modulation, azimuth frequency modulation, RCMC and the azimuth/range coupling. Since the term M is partially determined by the Doppler centroid, it may change with targets in different positions of the scene. Assuming that the attitude steering has been performed,

the f_{dc} equals zero, and M of the whole scene is the same as M_r. After RFM, the residual phase in the wave number domain is presented as:

$$\Theta_{re}(f_\tau, f_\eta) = \frac{-4\pi(f_0+f_\tau)}{c}\left[(R_c - R_r) - \frac{(P_1 - P_{1r})}{2}M^2 - \frac{(P_2 - P_{2r})}{3}M^3 - \frac{(P_3 - P_{3r})}{4}M^4 - \frac{(P_4 - P_{4r})}{5}M^5\right] \quad (21)$$

After RFM, the reference target can be focused well. However, the residual phase of the other targets away from reference position is still non-zero and is necessary to be corrected. The total RCM of each target in the scene can be separated into bulk and differential components. The bulk part, which is defined as the total RCM of the reference target, has been corrected in the RFM operation. The differential part, which can be corrected by interpolation in Range-Doppler domain, is then obtained by subtracting the bulk RCM from the total RCM. The differential RCM term in range time domain can be given as following according to Equation (17):

$$\mathrm{RCM}_{dif}(f_\eta) = -\left\{\frac{\lambda^2(P_1 - P_{1r})f_\eta^2}{8} - \frac{2\lambda^3(P_2 - P_{2r})f_\eta^3}{24} + \frac{3\lambda^4(P_3 - P_{3r})f_\eta^4}{64} - \frac{4\lambda^5(P_4 - P_{4r})f_\eta^5}{160}\right\} \quad (22)$$

A range IFFT is applied to transform the signal into RD domain after RFM, and the differential RCM can then be corrected by Sinc interpolation. Hence, RCMC of one target in RD domain effectively corrects the trajectory of a family of targets with the same slant range of closest approach.

Since the spaceborne SAR Doppler parameters are dependent on range elevation angle and the range swath of a Stripmap mode GeoSAR system is 300 km, the azimuth/range coupling term changes along with range direction. The 'bulk coupling-phase compensation' in the RFM operation cannot deal with the whole swath, and the data should be divided into several blocks. Provided that the whole range swath has been separated into N blocks, the residual azimuth/range coupling phase of each block after RFM can be presented as following:

$$\begin{aligned}\Theta_{coup}(r_c, f_r, f_\eta) = {} & [\Theta_5(r_c, f_\tau, f_\eta) - \Theta_5(r_{ref}, f_\tau, f_\eta)] \\ & - [\Theta_{\mathrm{RCM}}(r_c, f_\tau, f_\eta) - \Theta_{\mathrm{RCM}}(r_{ref}, f_\tau, f_\eta)] \\ & - [\Theta_a(r_c, f_\eta) - \Theta_a(r_{ref}, f_\eta)]\end{aligned} \quad (23)$$

where r_c means the slant range of one target in each data block, and r_{ref} the reference slant range of the target located at the

center of each data block. In traditional HRE-RDA case, the azimuth/range crossing coupling could be solved by compensating with SRC. The high order azimuth/range coupling of Geo-SAR needs to be appropriately compensated due to its super-long integration time. The signal after differential RCMC is transformed back into wave number domain through range FFT. Since the bulk azimuth/range coupling compensation has been performed in the RFM step, the residual part of each block can be compensated by the following filter:

$$H_{ci}(f_\tau, f_\eta) = \exp\{-j\Theta_{coup}(r_c, f_r, f_\eta)\}, \qquad (i = 1, 2, \ldots, N) \tag{24}$$

The signal is then transformed into RD domain through a range IFFT, and the residual azimuth phase term is compressed by a match filter as following.

$$H_a(\tau, f_\eta) = \exp\left\{-j\left[-\frac{4\pi(R_c - R_r)}{\lambda} + \frac{\pi\lambda(P_1 - P_{1r})f_\eta^2}{2} - \frac{\pi\lambda^2(P_2 - P_{2r})f_\eta^3}{6} + \frac{\pi\lambda^3(P_3 - P_{3r})f_\eta^4}{16} - \frac{\pi\lambda^4(P_4 - P_{4r})f_\eta^5}{40}\right]\right\} \tag{25}$$

Lastly, the signal is transformed into time domain by an azimuth IFFT. We can finally get a compressed complex image.

4. SIMULATION EXPERIMENTS

The capabilities of traditional RDA based on HRE and FDA depending on DRM-5 are compared in this section by simulation experiments. The simulation results are arranged as follows. Firstly, the necessity and superiority of DRM-5 for a Geo-SAR system is validated by comparing with HRE. Secondly, the residual azimuth/range coupling phase term and the range sub-swath blocking size is analyzed. Lastly, the performances of the two imaging algorithms are illustrated and compared. The simulation parameters are listed in Table 1.

4.1. Range Model Accuracy Comparison

The capabilities of range model (HRE and DRM-5) are determined by their accuracy, and the phase error of them can be calculated by subtracting the slant range values obtained by Equation (2). With respect to different orbital heights, the azimuth phase errors of HRE and DRM-5 are compared in Fig. 3. The spaceborne SAR for simulation, whose orbital inclination are 60° and latitude argument assumed 45°, has the azimuth resolution of 5 m. It is depicted that the performance of DRM-5, at the orbital altitudes lower than 36,000 km,

is very good compared with the 0.25π threshold line. However, the error of HRE is more than 0.25π when the satellite's height is higher than 6300 km.

Furthermore, a right-looking Stripmap mode Geo-SAR system, at 35,792 km orbital height, is employed to analyze the azimuth phase error properties of HRE and DRM-5. Three point targets are distributed across the range swath, and the interval between targets is 150 km. The simulation results are illustrated in Fig. 4, and the three targets are respectively marked as 'near, mid, and far'.

As depicted in Fig. 4, the maximum error of HRE during 620 s is around 280π, but this value of DRM-5 is lower than 0.05π. So DRM-5 will have a finer effect on Geo-SAR than HRE.

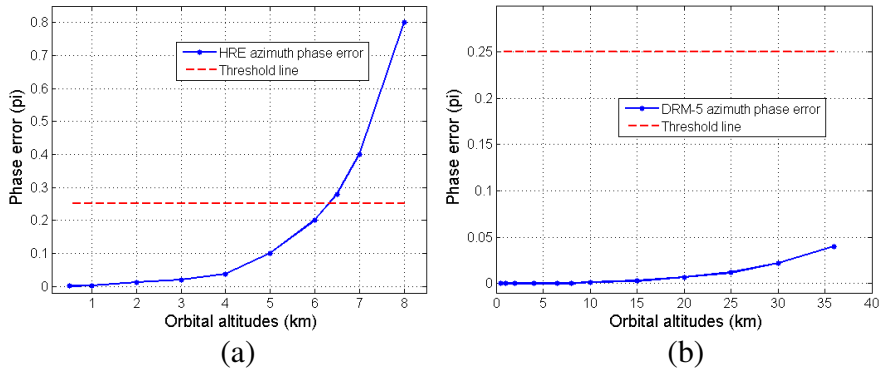

Figure 3. Azimuth phase error comparison between HRE and DRM-5 at different orbital altitudes. (a) HRE. (b) DRM-5.

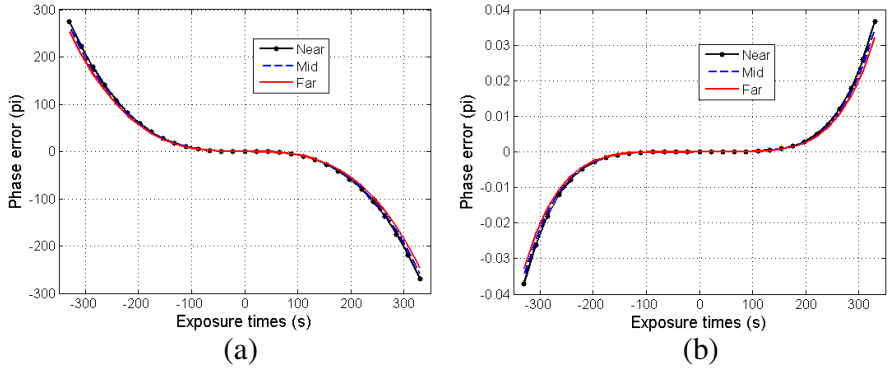

Figure 4. Azimuth phase error properties comparison between HRE and DRM-5 for Stripmap mode Geo-SAR. (a) HRE. (b) DRM-5.

4.2. Residual Azimuth/Range Coupling Phase Analysis and Data Blocking

In Geo-SAR condition, the varying Doppler parameters in the cross-azimuth direction should be considered clearly for the wide range swath. The high order azimuth/range coupling phase of the entire range swath data cannot be totally compensated by RFM. To process

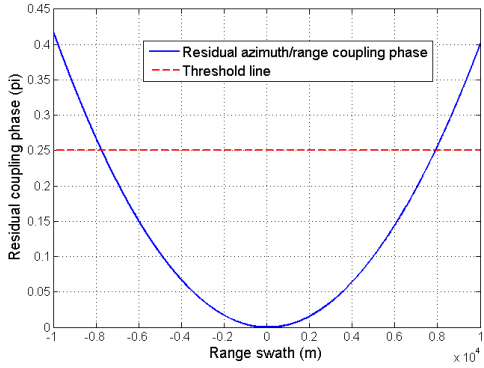

Figure 5. Residual azimuth/range coupling phase of Geo-SAR.

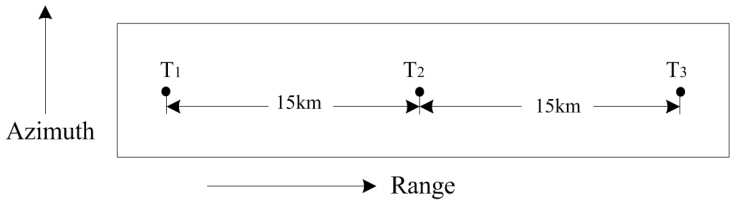

Figure 6. Three point targets in a 30 km scene.

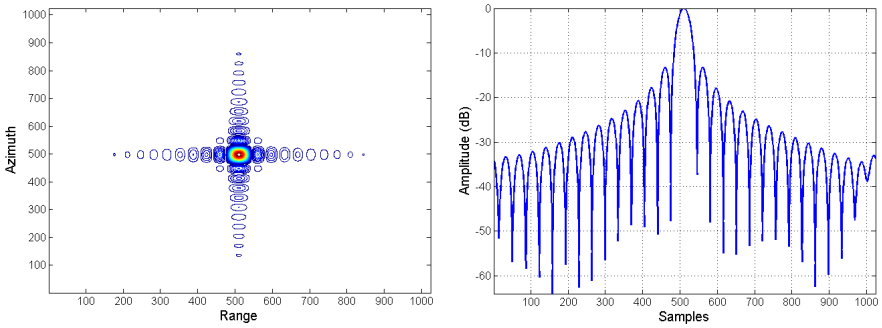

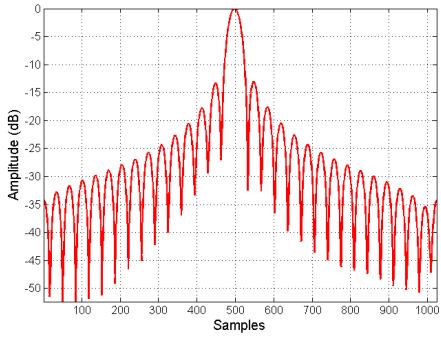

(c)

Figure 7. Focusing results of the center point target in the scene (30 km range swath). (a) T_2 contour plot. (b) T_2 range profile. (c) T_2 azimuth profile.

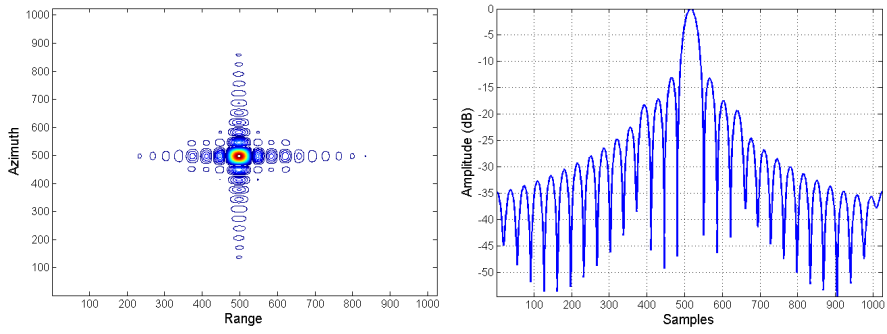

(a) (b)

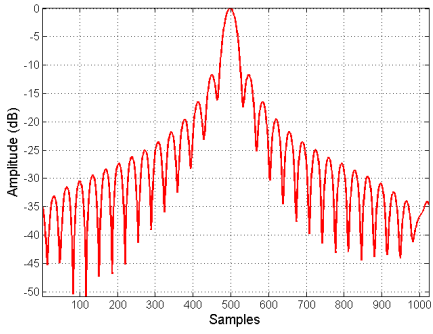

(c)

Figure 8. Focusing results of the far point target in the scene (30 km range swath). (a) T_3 contour plot. (b) T_3 range profile. (c) T_3 azimuth profile.

the data of a large scene, the whole data should be divided into several blocks along the range direction. After RFM, the residual azimuth/range coupling phase term of one single point target away from the reference position has been represented in expression (23). The largest residual azimuth/range coupling phase should be below the threshold 0.25π, and the size of the sub-block can be determined by it.

Figure 5 depicts that the residual coupling phase calculated by (23) is nonlinear along the cross-azimuth direction for Geo-SAR. The maximum data size that can be processed without blocking is around 15.8 km. Fig. 6 shows three point targets named as 'T_1, T_2 and T_3' which are located in a scene, and the scene size is 30 km (The interval between each target is 15 km). T_2 and T_3 are selected for focusing without blocking.

Figures 7 and 8 illustrate the performance of this new algorithm

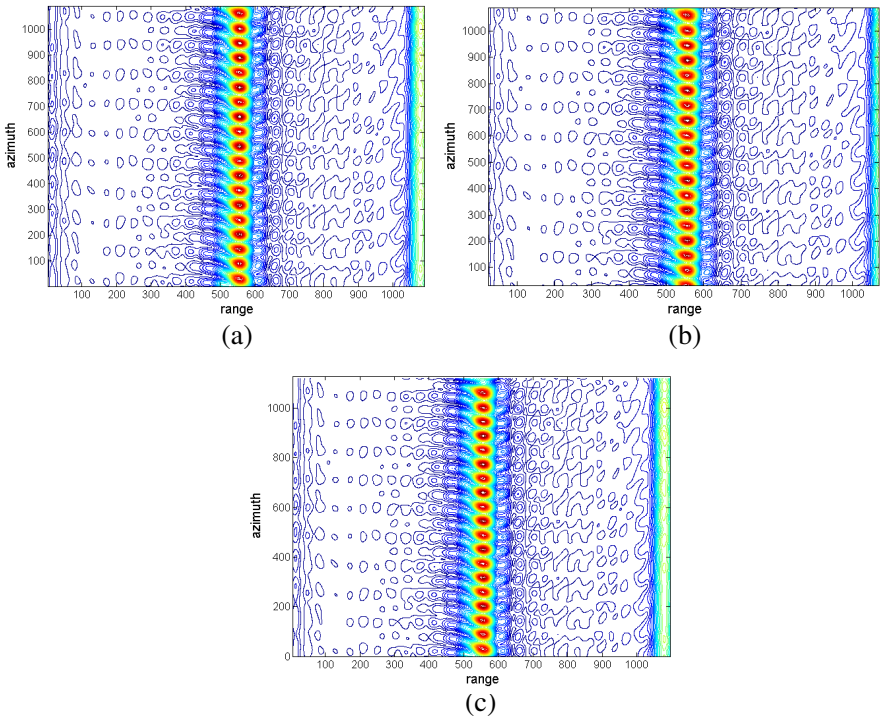

Figure 9. Geo-SAR signal processing by traditional RDA based on HRE (300 km range swath). (a) Near target contour plot. (b) Mid target contour plot. (c) Far target contour plot.

along the range direction without blocking by showing the contour plots and profiles of T_2 and T_3.

As depicted in Figs. 7 and 8, the target in the center of scene (T_2) can be focused well. However, the far one (T_3) suffers from a little defocused effect especially in azimuth direction.

As a result, the data after residual RCMC should be divided into several blocks in range direction, and the maximal remained coupling phase of each block should be under 0.25π. A 300 km range swath can be divided into 20 blocks and each block is 15 km in this paper. Range FT is applied to transform each sub-block data into wave number domain. The residual coupling phase term is then compensated according to (24), where the middle slant range of each block is defined as its reference slant range. Finally, the range IFT is applied to each block and the azimuth compression is performed for data focusing.

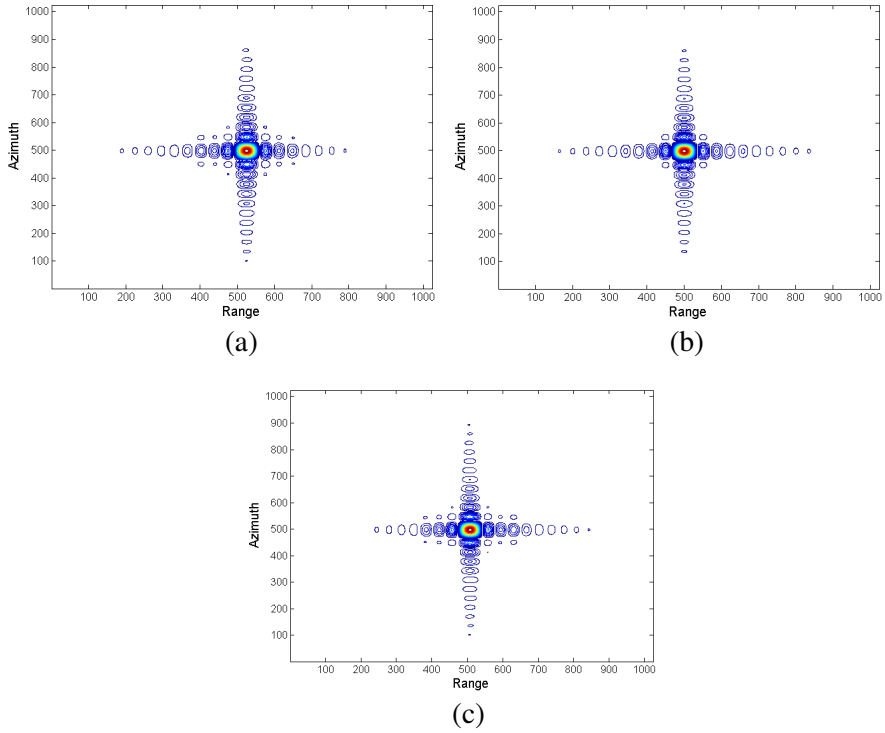

Figure 10. Geo-SAR signal processing by FDA based on DRM-5 (300 km range swath). (a) Near target contour plot. (b) Mid target contour plot. (c) Far target contour plot.

4.3. Imaging Algorithm Performance

A right-looking stripmap mode Geo-SAR system at a 35,792 km orbital altitude is employed for simulation. Without loss of generality, the satellite orbital position is assumed at the 45° latitude argument. The other simulation parameters are shown in Table 1. Three point targets (named as 'near', 'mid', and 'far' respectively like in Section 4.1) are focused in this section. They are distributed across the range swath in the azimuth beam center plane, and the space between them is 150 km. The single point target response should be interpolated in the vicinity of the peak since it is only represented by one or two samples in the large processed data. They are analyzed by selecting a 32×32 samples centered on the peak, and up-sampling by a factor of 32 to observe more clearly.

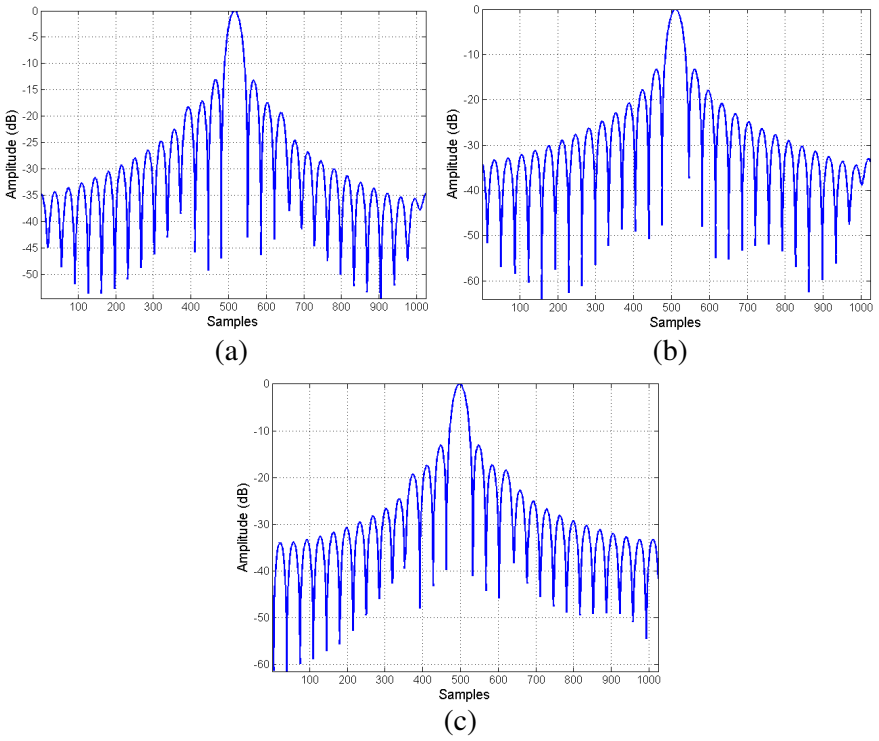

Figure 11. Range profiles of the three targets (near, mid and far) focused by FDA based on DRM-5 (300 km range swath). (a) Near target range profile. (b) Mid target range profile. (c) Far target range profile.

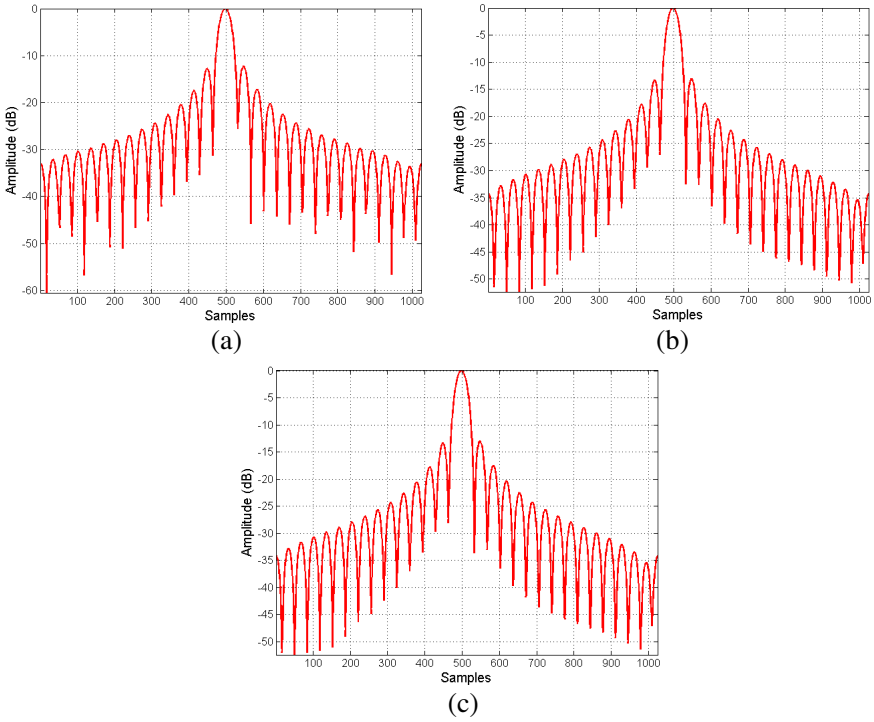

Figure 12. Azimuth profiles of the three targets (near, mid and far) focused by FDA based on DRM-5 (300 km range swath). (a) Near target azimuth profile. (b) Mid target azimuth profile. (c) Far target azimuth profile.

Figure 9 shows the contour plots of the three point targets along the range direction focused by traditional RDA based on HRE. They suffer from severe degradation and distortion, and can hardly be focused.

The raw echo signals of the point targets are processed by the novel FDA based on DRM-5, and their contour plots are given in Fig. 10 to verify the new imaging algorithm. All the targets can be focused well. These results are reasonable according to the conclusion in Section 4.1. The Azimuth and range profiles of the three targets compressed by FDA-DRM5 are given in Figs. 11 and 12. The well balanced sidelobe structure shows that they have been properly focused.

The three quality parameters: IRW (impulse response width), PSLR (peak sidelobe ratio) and ISLR (integrated sidelobe ratio) are shown in Table 2. They are close to the ideal values.

Table 2. Point target quality parameters.

	Range		
	IRW (m)	**PSLR (dB)**	**ISLR (dB)**
Target near	5.02	−13.29	−10.29
Target mid	5.02	−13.32	−10.25
Target far	5.03	−13.24	−10.20
	Azimuth		
	IRW (m)	**PSLR (dB)**	**ISLR (dB)**
Target near	5.03	−13.26	−10.19
Target mid	5.01	−13.36	−10.24
Target far	5.03	−13.22	−10.24

5. CONCLUSIONS

This paper represents a novel imaging algorithm (FDA) based on an accurate range model (DRM-5) to deal with the data of stripmap mode Geo-SAR. The DRM-5, employed to describe the slant range of Geo-SAR, is more accurate than the traditional HRE. The point target 2D RFS of DRM-5 is derived and expanded. Furthermore, a new Frequency Domain Algorithm (FDA) is proposed to cope with the data from stripmap mode Geo-SAR. To solve the varied Doppler parameters in the cross-azimuth direction, the whole 300 km range swath is blocked into 20 sub-segments. The high order azimuth/range coupling phase is compensated in each data block. According to the simulation results, the FDA based on DRM-5 has the efficiency and superiority on an L-band stripmap mode Geo-SAR system with an azimuth resolution around 5 m and 300 km range swath.

REFERENCES

1. Tomiyasu, K., "Synthetic aperture radar in geosynchronous orbit," *Proc. Antennas and Propagation Society International Symposium*, USA, May 1978.
2. Tomiyasu, K. and J. L. Pacell, "Synthetic aperture radar imaging from an inclined geosynchronous orbit," *IEEE Trans. Geosci. Remote Sens.*, Vol. 21, No. 3, 324–328, 1983.

3. Guo, D., H. Xu, and J. Li, "Extended wavenumber domain algorithm for highly squinted sliding spotlight SAR data processing," *Progress In Electromagnetics Research*, Vol. 114, 17–32, 2011.
4. Liu, Q., W. Hong, W. Tan, Y. Lin, Y. Wang, and Y. Wu, "An improved polar format algorithm with performance analysis for geosynchronous circular SAR 2D imaging," *Progress In Electromagnetics Research*, Vol. 119, 155–170, 2011.
5. Curlander, J. C. and R. N. McDonough, *Synthetic Aperture Radar: System and Signal Processing*, 565–591, Wiley, New York, 1991.
6. NASA and JPL, "Global earthquake satellite system: A 20-year plan to enable earthquake prediction," JPL Document, 400–1069, March 2003.
7. Wei, S.-J., X.-L. Zhang, and J. Shi, "Linear array SAR imaging via compressed sensing," *Progress In Electromagnetics Research*, Vol. 117, 299–319, 2011.
8. Xu, W., P. Huang, and Y.-K. Deng, "Muti-channel SPCMB-TOPS SAR for high-resolution wide-swath imaging," *Progress In Electromagnetics Research*, Vol. 116, 533–551, 2011.
9. Moreira, A. and Y. Huang, "Airborne SAR processing of highly squinted data using a chirp scaling approach with integrated motion compensation," *IEEE Trans. Geosci. Remote Sens.*, Vol. 32, No. 5, 1029–1040, 1994.
10. Eldhuset, K., "A new fourth-order processing algorithm for spaceborne SAR," *IEEE Trans. Aero. Electronic Sys.*, Vol. 34, No. 3, 824–835, 1998.
11. Eldhuset, K., "Spaceborne bistatic SAR processing using the EETF4 algorithm," *IEEE Geosci. Remote Sens. Lett.*, Vol. 6, No. 2, 194–198, 2009.
12. Neo, Y. L., F. Wong, and I. G. Cumming, "A two dimensional spectrum for bistatic SAR processing using series reversion," *IEEE Geosci. Remote Sens. Lett.*, Vol. 4, No. 1, 93–96, 2007.
13. Pillai, S. U., B. Himed, and K. Y. Li, "Effect of Earth's rotation and range foldover on space-based radar performance," *IEEE Trans. Aero. Electronic Sys.*, Vol. 42, No. 3, 917–932, 2006.
14. Zhao, B., X. Qi, D. Yu-Kai, R. Wang, and H. Song, "Accurate fourth-order doppler parameter estimation approach for geosynchronous SAR," *Proc. EUSAR 2012*, Nürnberg, Germany, 2012.

15. Zhao, B., X. Qi, H. Song, W. Gao, X. Han, and R. P. Chen, "The accurate fourth-order doppler parameter calculation and analysis for geosynchronous SAR," *Progress In Electromagnetics Research*, Vol. 140, 91–104, 2013.
16. Wu, C., K. Y. Liu, and M. J. Jin, "A modeling and correlation algorithm for spaceborne SAR signals," *IEEE Trans. Aero. Electronic Sys.*, Vol. 18, No. 5, 563–574, 1982.
17. Davidson, G. W., I. G. Cumming, and M. R. Ito, "A chirp scaling approach for processing squint mode SAR data," *IEEE Trans. Aero. Electronic Sys.*, Vol. 32, No. 1, 121–133, 1996.
18. Bamler, R., "A comparison of range-Doppler and wavenumber domain SAR focusing algorithm," *IEEE Trans. Geosci. Remote Sens.*, Vol. 30, No. 4, 706–713, 1992.
19. Tan, W., W. Hong, Y. Wang, and Y. Wu, "A novel spherical-wave three-dimensional imaging algorithm for microwave cylindrical scanning geometries," *Progress In Electromagnetics Research*, Vol. 111, 43–70, 2011.
20. Zhang, M., Y. W. Zhao, H. Chen, and W.-Q. Jiang, "SAR imaging simulation for composite model of ship on dynamic ocean scene," *Progress In Electromagnetics Research,* Vol. 113, 395–412, 2011.
21. Zhao, B., X. Qi, Y. Deng, R. Wang, H. Song, and Y. Luo, "A new method of improving the accuracy of the hyperbolic range equation," *Proc. IGARSS 2012*, Munich, Germany, 2012.
22. Fielder, H., E. Boerner, J. Mittermayer, and G. Krieger, "Total zero Doppler steering: A new method for minimizing the Doppler centroid," *IEEE Geosci. Remote Sens. Lett.*, Vol. 2, No. 2, 141–145, 2005.